Quantifying the origin of the antibacterial activity of nanosilver

[1]Georgios A. Sotiriou, [2]Andreas Meyer, [1]Jesper T.N. Knijnenburg, [2]Sven Panke and [1]Sotiris E. Pratsinis

[1]Particle Technology Laboratory, [2]Bioprocess Laboratory, Institute of Process Engineering
Department of Mechanical and Process Engineering
Swiss Federal Institute of Technology
Zurich (ETH Zurich)

ABSTRACT

The antibacterial activity of nanosilver against Gram negative *Escherichia coli* bacteria is investigated by immobilizing nanosilver on nanostructured silica particles and closely controlling Ag content and size. These Ag/SiO_2 nanoparticles were characterized by S/TEM, EDX spectroscopy, X-ray diffraction. The antibacterical activity of these composite samples was investigated for a constant composite particle concentration. The highest activity was observed for the higher silver content particles.

.

Keywords: silver, silica, nanoparticles, antibacterial, SSA

1 INTRODUCTION

Silver (Ag) is a metal known to humans since the ancient times. It is considered a precious metal, and it can conduct electricity and heat better than any other metal. Silver has been used since antiquity in several applications such as coins, jewelry and silverware, till the latest years in many other fields, such as in photography, explosives, as dental alloys [1, 2]. Silver's ability to kill microorganisms is also known for many years. The mechanism responsible for silver's antibacterial ability is not yet fully understood. Feng *et al.* [3] investigated the effect of Ag^+ on bacteria cells, reaching the conclusion that Ag^+ intefere with DNA replication. Morones *et al.* [4] investigated the activity of silver nanoparticles against bacteria and proposed that silver nanoparticles damage the integrity of the cell membrane and may penetrate into the interior. In doing so, they interact with and possibly destroy sulfur or phosphorus containing compounds (such as DNA), that are vital for the cell. Furthermore, Morones and coworkers suggest that the Ag nanoparticles release Ag^+ from their surface, contributing additionally to the antibacterial properties. Lok *et al.* [5] found that the parameter that affects silver's antibacterial property is the Ag^+ which are chemisorbed on the surface of the metallic silver nanoparticles. Zero-valent silver nanoparticles have no antibacterial activity, while the partially surface oxidized silver nanoparticles exhibit antibacterial activity, due to the chemisorbed Ag^+ on their surface.[6, 7]

There are several studies on the antibacterial activity of nanosilver made by wet-methods [5, 8], and flame spray pyrolysis [6, 9]. Smaller nanosilver particles are more toxic than larger ones [5] especially when oxidized [5, 9]. Additionally, even though silver metal is practically insoluble in water [10], when present in nanometer size range Ag^+ ions are released (leached) [9, 11, 12] from its surface. It has been shown recently [6] that the antibacterial activity of small (<10 nm) nanosilver particles is dominated by Ag^+ ions, while for larger ones (>15 nm) the antibacterial contribution by Ag^+ ions and particles is comparable. Such a behavior implies a surface area dependency of the antibacterial activity especially for small nanosilver sizes since the Ag^+ ion release is proportional to the exposed nanosilver surface area [6]. Additionally, when a nanothin silica coating on the surface of nanosilver is applied, this antibacterial activity can be minimized [13, 14]. One way to stabilize the Ag nanoparticles is to attach them on a support material, such as silica. Therefore, by doping silver nanoparticles on a silica matrix the problems of aggregation are overcome, while their antibacterial properties are maintained. Most methods for the synthesis of silver/silica nanocomposites involve wet phase synthetic routes, with the most well known the sol-gel method [15, 16]. However, most of the wet synthetic routes are time-consuming, they involve multiple steps processes and there are limitations in the scalability [17].

Flame synthesis is one of the established commercial processes for making inexpensive ceramic nanoparticles [18]. Recently, a relatively new technique, the so called flame spray pyrolysis (FSP), has been developed, which uses liquid precursor solutions and is applicable for the synthesis of a broad range of products including metal oxides, mixed metal oxides and metals on metal oxides [19]. The synthesis of silver nanoparticles doped on ZnO has been reported with FSP, used for photocatalytic applications [20]. Additionally, silver/silica nanoparticles have been produced by FSP, and their catalytic activity was tested, as well as their antimicrobial and antifungal properties [21, 22]. However, there has not been any study investigating the precursor selection effects on the morphology of the product particles, as well as the correlation between the silver content and the antibacterial activity.

2 EXPERIMENTAL

2.1 Particle synthesis

Silver nitrate (Fluka, purity >99%) and hexamethyldisiloxane (HMDSO, Aldrich, purity >97%)

were used as silver and silicon precursors, respectively. Appropriate amount of silver nitrate was dissolved in ethanol (Alcosuisse) and diethylene glycolmonobutyl ether (Fluka, purity >98%), both at a volume ratio 1:1, and stirred at room temperature for 3 hours. The corresponding amount of HMDSO for a given *xAg/SiO₂* product was added and stirred for a few minutes just before that solution was fed into the FSP setup. The total metal (Ag and Si) concentration was 0.5 M. Particles were made by flame spray pyrolysis (FSP) as described elsewhere [23]. The precursor solution was fed through the FSP capillary nozzle at a rate 5 ml/min and dispersed by 5 l/min oxygen (Pan Gas, purity >99%). The weight fraction of the Ag in the Ag/SiO_2 product ranged from 0 to 25 wt%. The notation for the different particles is: *xAg/SiO₂*, for a concentration of *x wt%* of Ag in the final product.

2.2 Particle characterization

Scanning transmission electron microscopy (STEM) on a Tecnai F30 (FEI; field emission gun, operated at 300 kV). The STEM images were recorded with a high-angle annular dark field (HAADF) detector revealing the Ag particles with bright contrast (Z contrast). The electron beam could be set to selected areas to determine material composition by energy dispersive X-ray spectroscopy (EDXS; detector (EDAX) attached to the Tecnai F30 microscope). Product particles were dispersed in ethanol and deposited onto a perforated carbon foil supported on a copper grid.
The crystallite size of silver was determined by XRD [23] using the TOPAS 3 software and the Rietveld method and fitting only its (111) main diffraction peak (2θ = 36°-40°) with the Inorganic Crystal Database [ICSD Coll. Code.: 064995]. The Brunauer-Emmett-Teller (BET) specific surface area (*SSA*) of the particles was measured by five-point nitrogen adsorption.

2.3 Antibacterial evaluation

A growth inhibition assay was performed to examine the antibacterial activity of the Ag/SiO_2 nanoparticles. To do so, *E. coli* JM101 bacteria synthesizing a green fluorescent protein (GFP) from a plasmid-encoded gene were grown in Luria-Bertani (LB) broth at 37 °C overnight. The culture was subsequently diluted with LB to an optical density (OD) at 600 nm of 0.05, which corresponds to approximately 10^7 colony forming units (CFU)/ml. The Ag/SiO_2 nanoparticles were dispersed in de-ionized water using ultrasonication (Sonics vibra-cell) for 20 seconds at 75% amplitude with a pulse configuration on/off of 0.5s/0.5s. After ultrasonication, the nanoparticles were homogeneously dispersed and stable in the aqueous solution. For the assay, 50 µl of the aqueous solutions containing the dispersed Ag/SiO_2 nanoparticles were added to 50 µl of the diluted cells. The error bars for each data point were obtained as the standard deviation of 4 measurements.

3 RESULTS & DISCUSSION

3.1 Particle morphology

Figure 1 shows the *10Ag/SiO₂* sample. The Ag clusters are revealed by the bright contrast. There is a bimodality of the Ag clusters. This bimodal particle size distribution is consistent with X-ray diffraction (XRD) analysis. Figure 2a shows the XRD spectra of the *10Ag/SiO₂* and *25Ag/SiO₂* samples. The peak positions indicated by the squares correspond to (111), (200) and (220) crystal planes of Ag metal (ICSD nr. 064995). By Rietveld analysis on the (111) peak, two crystal modes were obtained with the following average crystal sizes and mass fractions (wt%): For the *10Ag/SiO₂* sample, they were 7.4 ± 1.7 nm (81%) and 37.1 ± 14 nm (19%) while for the *25Ag/SiO₂* 9.4 ± 1.9 (79%) and 57.8 ± 19.6 (21%).
The bimodal cluster size distribution is attributed to partial evaporation of spray droplets during FSP. So fine Ag clusters are made by gas-to-particle conversion of the precursor vapor, while larger ones come from droplet-to-particle conversion during Ag precipitation in larger precursor droplets prior to their complete evaporation and combustion [24]. For lower Ag contents, the crystal concentration was below the XRD detection limit and thus only a broad band corresponding to amorphous SiO_2 was obtained. No peaks corresponding to Ag_2O (triangles) or AgO (circles) (ICDS nrs. 202055 and 031058, respectively) oxides were found, even though Ag nanoparticles produced by FSP have their surface partially oxidized [21].

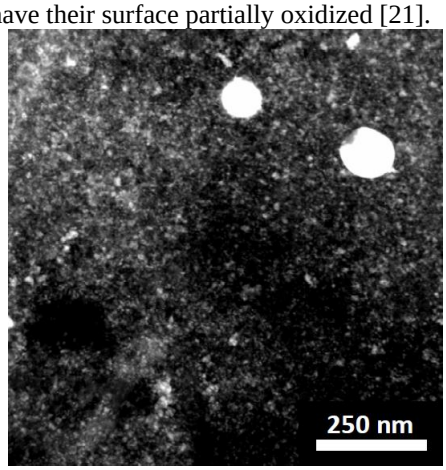

Figure 1. STEM image of *10Ag/SiO₂* with a broad distribution of Ag clusters comprising two modes (inset): a fine one for clusters made by gas-to-particle conversion and a larger one for clusters made by droplet-to-particle conversion.

Figure 2b shows the specific surface area (*SSA*) of Ag/SiO_2 (circles) and SiO_2 (triangles) as a function of the Ag content of these particles. Both the *SSA* and that of SiO_2 alone are increasing for $x \leq 2$ wt%. The presence of Ag in the product affects the growth of SiO_2, perhaps by formation of a solid

solution at very low Ag contents, as it has been observed also with trace contents of SiO_2-based mixed oxides [25]. However, as soon as the Ag content is above 2 wt%, the *SSA* decreases while that of pure SiO_2 (triangles) remains virtually intact. At these contents, Ag stops influencing SiO_2 formation and precipitates on its surface further downstream given the difference in boiling points [26] between Ag and SiO_2, as with FSP synthesis of noble metal clusters on ceramic supports [27]. Therefore, the overall *SSA* of the Ag/SiO_2 nanoparticles is attributed mainly to SiO_2.

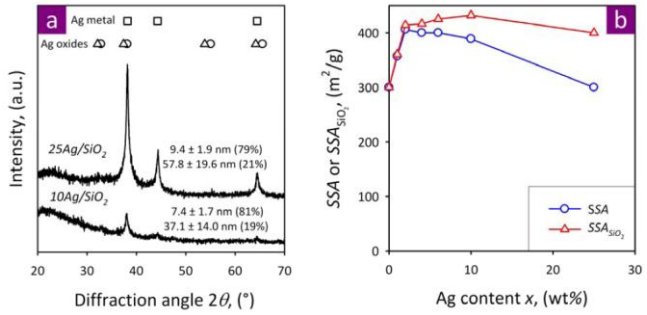

Figure 2. (a) XRD spectra of *10* and *25Ag/SiO₂* nanoparticles. The peak position of the Ag metal (squares) and oxides Ag_2O (triangles) or AgO (circles) are shown also. For each spectrum, two average crystal sizes with their uncertainties and mass fractions (wt%) corresponding to two crystal modes are listed. (b) The overall Ag/SiO_2 (circles) particle specific surface area (*SSA*) and the one of SiO_2 (SSA_{SiO2}, triangles) is presented as a function of the Ag content, *x*. As the SSA_{SiO2} does not change with Ag content, the Ag presence does not affect the surface of the silica support for $x > 2$ wt%.

3.2 Antibacterial activity

The antibacterial effect of the samples produced from the precursor solution containing Ag nitrate-HMDSO was examined against the Gram-negative bacterium *E. coli*. In Figure 6, the fluorescence of *E. coli* cultures synthesizing GFP at 37 °C in the presence of the Ag/SiO_2 nanoparticles is presented as a function of time, representing the growth of the strain under the different experimental conditions. Figure 6 shows the results from the investigation of the effect of the Ag content (0 – 25 wt %), keeping the particle concentration constant (8 μg/ml), as well as the error bar for the last data point. It can be seen that pure SiO_2 particles do not affect the growth of the bacteria. However, in the presence of the Ag-containing SiO_2 particles, the antibacterial effect is increased with an increased Ag content. No growth at all after 5.5 hours is observed for the *25Ag/SiO₂* particles, for the same concentration of 8 μg/ml. This concentration corresponds to 2 μg/ml of Ag.

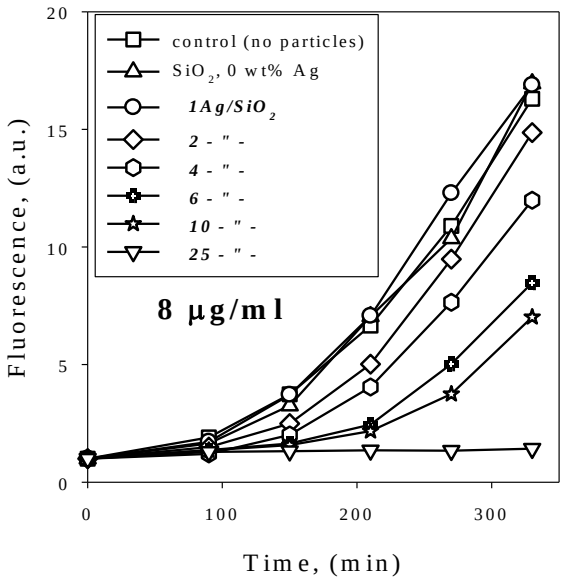

Figure 3: The growth curves in the presence of the different Ag content particles (0 – 25 wt %), for the same concentration of 8 μg/ml.

Taking into account the possible responsible mechanisms for the antibacterial activity of Ag nanoparticles, it is suggested that the *Ag SSA* plays an important role. In the case of the Ag's ability to damage vital compounds on the membrane or even compounds inside the cell, it is of highest importance to increase the contact of the Ag nanoparticles with these compounds, and thus to increase the *Ag SSA*. In the case of the Ag^+ being released from the Ag's surface, also the higher *Ag SSA*, the more Ag^+ would be released, making the Ag particles with the highest *Ag SSA* the most effective ones. Therefore, it is of major importance to control the accessibility of the *Ag SSA* for such an effect of the Ag/SiO_2 nanoparticles, which could be incorporated in polymer matrixes and other composites or be deposited to surfaces, for an antibacterial use. Therefore, it should be the *Ag SSA* which would indicate the antibacterial activity of the Ag nanoparticles. Figure 4 shows the amount of cultivable bacteria after 5.5 hours at 37 °C, in the presence of all the different Ag content particles. However, this time the total particle concentration has been normalized in respect to the Ag surface area. Therefore, all the data are in the presence of the same amount of Ag surface area ($5.5 \cdot 10^{-6}$ m^2/ml) for all the samples, apart from the sample containing only SiO_2. It can be observed that for pure SiO_2, the amount of cultivable bacteria is the same as if no particles are present (as observed from Fig. 3), however, all the rest data have similar values, indicating that the antibacterial effect is identical in all cases. This leads to the conclusion that the mechanism responsible for the antibacterial activity is strongly surface area dependent.

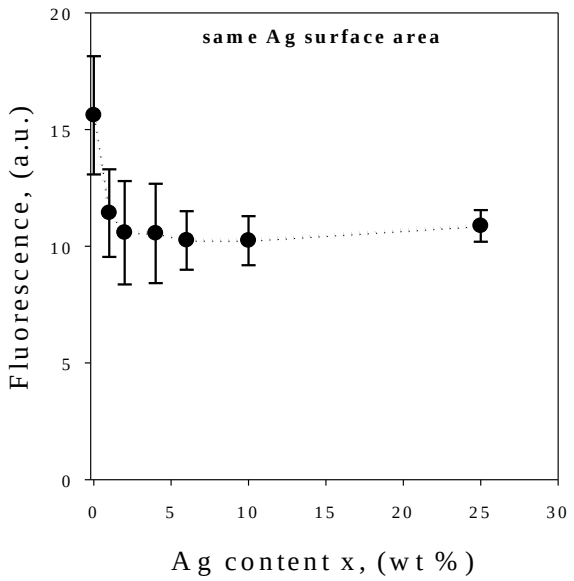

Figure 4: The growth curves of the bacteria at 37 °C, in the presence of all the different Ag content particles on the basis of equivalent Ag surface area.

4 CONCLUSIONS

Silver nanoparticles dispersed within amorphous silica have been synthesized using FSP. Different precursor solutions have been examined, and their effects on the final product particles have been investigated. Particle size and particle size homogeneity can be tuned depending on the precursor solution. Additionally, the amount of the Ag surface area which is exposed and not embedded within the amorphous SiO_2 matrix (*Ag SSA*) depends on the Ag precursor used. Higher values of the *Ag SSA* were obtained for Ag precursors with higher decomposition point. The antibacterial activity of the produced nanoparticles was also investigated. There was a more enhanced antibacterial effect for an increased mass dose, in the presence of the same particles. Finally, the strong Ag surface area dependency of the antibacterial activity was demonstrated by investigating the growth curves of the bacteria in the presence of the produced particles, on the basis of equivalent *Ag SSA* concentrations, though.

REFERENCES

[1] X. Chen, H. J. Schluesener, *Toxicol. Lett.* **2008**, *176*, 1.
[2] D. M. K. Lam, B. W. Rossiter, *Scientific American* **1991**, *265*, 48.
[3] Q. L. Feng, J. Wu, G. Q. Chen, F. Z. Cui, T. N. Kim, J. O. Kim, *J. Biomed. Mater. Res.* **2000**, *52*, 662.
[4] J. R. Morones, J. L. Elechiguerra, A. Camacho, K. Holt, J. B. Kouri, J. T. Ramirez, M. J. Yacaman, *Nanotechnology* **2005**, *16*, 2346.
[5] C. N. Lok, C. M. Ho, R. Chen, Q. Y. He, W. Y. Yu, H. Sun, P. K. H. Tam, J. F. Chiu, C. M. Che, *J. Biol. Inorg. Chem.* **2007**, *12*, 527.
[6] G. A. Sotiriou, S. E. Pratsinis, *Environ. Sci. Technol.* **2010**, *44*, 5649.
[7] G. A. Sotiriou, A. Teleki, A. Camenzind, F. Krumeich, A. Meyer, S. Panke, S. E. Pratsinis, *Chem. Eng. J.* **2011**, *170*, 547.
[8] P. Li, J. Li, C. Z. Wu, Q. S. Wu, *Nanotechnology* **2005**, *16*, 1912.
[9] C. Gunawan, W. Y. Teoh, C. P. Marquis, J. Lifia, R. Amal, *Small* **2009**, *5*, 341.
[10] D. R. Lide, *CRC Handbook of Chemistry and Physics*, CRC Press/Taylor and Francis, Boca Raton, FL **2010**.
[11] T. M. Benn, P. Westerhoff, *Environ. Sci. Technol.* **2008**, *42*, 4133.
[12] E. Navarro, F. Piccapietra, B. Wagner, F. Marconi, R. Kaegi, N. Odzak, L. Sigg, R. Behra, *Environ. Sci. Technol.* **2008**, *42*, 8959.
[13] G. A. Sotiriou, A. M. Hirt, P. Y. Lozach, A. Teleki, F. Krumeich, S. E. Pratsinis, *Chem. Mater.* **2011**, *23*, 1985.
[14] G. A. Sotiriou, T. Sannomiya, A. Teleki, F. Krumeich, J. Vörös, S. E. Pratsinis, *Adv. Funct. Mater.* **2010**, *20*, 4250.
[15] C. Baker, A. Pradhan, L. Pakstis, D. J. Pochan, S. I. Shah, *J. Nanosci. Nanotechnol.* **2005**, *5*, 244.
[16] Y. H. Kim, D. K. Lee, H. G. Cha, C. W. Kim, Y. S. Kang, *J. Phys. Chem. C* **2007**, *111*, 3629.
[17] G. A. Sotiriou, S. E. Pratsinis, *Curr. Opin. Chem. Eng.* **2011**, *1*, 3.
[18] S. E. Pratsinis, *Prog. Energ. Combust. Sci.* **1998**, *24*, 197.
[19] L. Madler, H. K. Kammler, R. Mueller, S. E. Pratsinis, *J. Aerosol. Sci.* **2002**, *33*, 369.
[20] M. J. Height, S. E. Pratsinis, O. Mekasuwandumrong, P. Praserthdam, *Appl. Catal. B-Environ.* **2006**, *63*, 305.
[21] S. Hannemann, J. D. Grunwaldt, F. Krumeich, P. Kappen, A. Baiker, *Appl. Surf. Sci.* **2006**, *252*, 7862.
[22] M. J. Height, S. E. Pratsinis, *Switzerland Patent*, **2007**.
[23] L. Madler, W. J. Stark, S. E. Pratsinis, *J. Mater. Res.* **2003**, *18*, 115.
[24] L. Madler, S. E. Pratsinis, *J. Am. Ceram. Soc.* **2002**, *85*, 1713.
[25] H. Schulz, L. Madler, S. E. Pratsinis, P. Burtscher, N. Moszner, *Adv. Funct. Mater.* **2005**, *15*, 830.
[26] D. R. Lide, *CRC Handbook of Chemistry and Physics*, CRC Press/Taylor and Francis, Boca Raton, FL **2009**.
[27] R. Strobel, S. E. Pratsinis, *J. Mater. Chem.* **2007**, *17*, 4743.